ADVANCED FUNCTIONAL MATERIALS
www.afm-journal.de

ZnO/PVA Macroscopic Fibers Bearing Anisotropic Photonic Properties

Natacha Kinadjian, Marie-France Achard, Beatriz Julián-López, Maryse Maugey, Philippe Poulin, Eric Prouzet, and Rénal Backov**

This manuscript is dedicated to Professor Purificación Escribano

Composite PVA/ZnO-nanorods fibers, synthesized through co-axial flux extrusion exhibit higher anisotropic photonic properties, both in absorption and emission, as a result of the collective alignment of the ZnO nanorods along the main axis of the PVA fiber. This photonic anisotropy is triggered by a synergistic interaction between the PVA matrix, stretched above the glass transition temperature (Tg), and cooled down under strain. Compared with non-elongated fibers that present an isotropic emission, composite fibers previously submitted to a tensile stress absorb selectively UV emission when the polarized laser beam is parallel to the main axis of the fiber. In addition, their photolumincescence is also anisotropic, with a waveguide behavior along the main axis of the fiber. Mechanical properties of these composite fibers are also drastically improved, compared with pure PVA fibers: the longitudinal Young modulus of these fibers is increased from 2 to 6 GPa upon ZnO addition, a value similar to those already observed for composite fibers, prepared either with carbon nanotubes, or V_2O_5 macroscopic fibers.

1. Introduction

Zinc oxide, with a wide direct band gap of 3.37 eV and high exciton binding energy (60 meV) larger than the thermal energy at room temperature,[1] represents intrinsically a promising material for ultra-violet nano-optoelectronic devices and lasers operating at room temperature.[2] Considering the morphology of ZnO, a tremendous amount of nanostructures have been obtained ranging from nanowires,[3] nanorods,[4] nanobelts,[5] nanotubes,[6] aligned nanonails,[7] and so forth. Properties of ZnO regarding the absorption and emission properties are well-known,[8] but it is interesting to check if the expected emission polarization predicted from modeling,[9] can be observed for ZnO anisotropic structures. As measurements on a single nanorod are difficult,[10] being able to align a whole population of ZnO nanorods along a single axis, is a better way to evaluate the macroscopic effect of collective alignment. As a result, beyond the specific interest of validating anisotropic properties provided by shape anisotropy at the nano-scale, actual functionality can result from a magnification of this local property by providing the correct synergy among a collection of nanoparticles through preferential orientation, and true applications can result from this magnification if the design and processing of these synergistic nanostructures is easy. It has been demonstrated that a multiplexed combination of chemistry, physical chemistry of complex fluids, and biomimetic processes is a suitable way to define specific synthetic pathways that allow us to reach multi-scale architectures bearing functionalities. These methods, which have been widely used for many years, can be summarized under the "*Integrative Chemistry*" definition,[11] an extension of the previous concept of integrative syntheses,[12] which allows for designing and engineering advanced functional hierarchical architectures, as demonstrated in many examples.[13,14] More specifically, the association of micro-extrusion and gelling mechanisms, allowed us to achieve the preparation of carbon nanotubes,[15] and vanadium oxide macroscopic containing composite fibers.[14,16,17] In this study, we report on a new method for the preparation of PVA/ZnO-nanorods composite fibers. We demonstrate that the additional order resulting from the micro-extrusion and specific post-alignment, provides an additional level of anisotropy photonic properties as a result of an optimized alignment of the ZnO nanorods within the fibers. This process, illustrates how intrinsic properties of anisotropic nanostructures can be

N. Kinadjian, M.-F. Achard, M. Maugey, P. Poulin, R. Backov
Centre de Recherche Paul Pascal
office 115, UPR 8641-CNRS,
115 Avenue Albert Schweitzer, 33600 Pessac, France
Phone: 33 556 845630, FAX: 33 556 845600
E-mail: backov@crpp-bordeaux.cnrs.fr

B. Julián-López
Department of organic and inorganic chemistry ESTCE - Universitat Jaume I. Avda. Sos Baynat s/n, 12071 Castellón, Spain
Phone: 34 964 728234, FAX: 34 964 728214
E-mail: julian@qio.uji.es

N. Kinadjian, E. Prouzet
Department of Chemistry & Waterloo Institute of Nanotechnology
University of Waterloo
200 University Avenue West, Waterloo, Ontario, Canada N2L 3G1
FAX: +1 519 746 0435
E-mail: eprouzet@uwaterloo.ca

DOI: 10.1002/adfm.201200360

magnified by collective properties resulting from a judicious hierarchical structure.

2. Experimental Section

Materials: $ZnCl_2.H_2O$, $N_2H_4.H_2O$, Poly-Vinyl alcohol PVA (Mw 120 000, hydrolysed, 87–89%) and Na_2SO_4 were purchased from Aldrich and used as received.

Syntheses: *ZnO nanorods syntheses*: The synthesis of ZnO nanorods was inspired from Zhu et al.[18]Typically, 0.95 g of $ZnCl_2$ and 0.75 ml of $N_2H_4.H_2O$ were added to 160 ml of distilled water under stirring. A slurry-like white precipitate was formed. Once the solution became homogeneous, it was transferred into a Teflon-lined stainless steel autoclave of 120 ml capacity and sealed. The autoclave was maintained at 200 °C for 24 h and cooled down through the autoclave inertia. The solution was removed and washed several times with distilled water. A maximum of supernatant water was removed and the remaining sol was transferred into a sample bottle. The zinc oxide sol weight fraction was determined through dry extracts. Solid polyvinylalcohol (PVA) was then added into the solution under stirring was kept for 24 hours until the PVA was fully dissolved. Finally, the excess of PVA beads was filtered out, and the final PVA weight fraction was determined through dry extracts.

ZnO/PVA co-extrusion process: The fibers were generated by needle injection of the as-prepared PVA/ZnO dispersion into a rotating bath containing a saturated salt solution of Na_2SO_4. The extrusion was maintained tangential to the rotation axis of the beaker in order to promote a pseudo-coaxial flux at the external part of the syringe hole. The diameter of the spinneret is 300 µm. The beaker containing the salt solution was kept at constant rotation of 25 rpm, while the solution containing the PVA/ZnO dispersion was extruded out of the syringe at a constant flux of 40 $ml.h^{-1}$. Upon the completion of the extrusion process, the ZnO/PVA fibers were meticulously taken out of the beaker by hand and allowed to dry in air. Finally, the fibers were washed once in water to remove the excess of salt. We would like to mention that the polymer in use should be soluble in water while bearing OH group to promote hydrogen bond with the hydroxyl pending group at the inorganic particles external surface. Thereby PVA partially hydrolyzed is appearing as the polymer of choice in this extrusion process.

ZnO fibers extension process: Stretch under load of the fibers was performed with a ZWICK/ROELL Z2.5 apparatus at a constant traction speed of 1 mm/min. The fibers were maintained largely above PVA glass transition (T_g = 85 °C) during the mechanical extension processes.

Characterization: Morphological analysis of the particles was carried out by Transmission Electron microscopy (TEM) with a JEOL JSM-840, the samples being placed on a grid and carbon-coated prior examination. Scanning Electron Microscopy (SEM) observations performed at 15 kV on a TM3000 Hitachi apparatus allowed us to evaluate the ZnO particles repartition within the fibers. The crystalline structure of ZnO was characterized by XRD with a PANalytical X'pert MDP with a Bragg-Brentano θ–θ geometry, equipped with a back graphite monochromator, a spinner and a 3 × 15 positions sample holder (CuK_α X-ray, λ = 1.54 Å – 40 kV working voltage, 40 mA working intensity). Studies of the ZnO particles alignment inside the fibers, were performed with a homemade X-ray scattering apparatus equipped with a microfocus copper rotating anode X-ray source (Rigaku MicroMax-007 HF) combined with multi-layers optics and a 3-pinholes collimation, the sample holder being mounted on a X-Y stage. Individual fibers were vertically placed on off-centered supports, with the fiber main axis perpendicular to the X-ray beam. The scattering signal was collected on a 2-dimensional detector (Image plate from Mar Research). In the present work, the sample-detector distance was fixed to 103 mm in order to record in parallel the Bragg reflections over a 0–40 degree 2-theta angular range. Silver behenate was used as a reference. The anisotropic angular distribution of ZnO crystals in the fibers was quantified by integrating first the radial intensity of the (001) diffraction line, and report this intensity as a function of the [(–100) – (+80)] degree angular orientation on the 2D detector, zero being located at the position of the maximum intensity. This analysis was applied to fibers prepared under various stretching constraints, and the quantification of the anisotropy was achieved by fitting the previous angular-dependent intensities with a Lorentzian function, the anisotropy factor being further reported as the full width at half maximum (FWHM). It results that a higher anisotropy will appear with a narrower distribution of the diffracted intensity on the 2D detector, hence a small FWHM. Therefore, this value represents the angular distribution of the particles axes around the fiber axis and allows for quantifying the particles orientation inside the fiber. Characterization of the fibers mechanical properties was carried out with a ZWICK/ROELL Z2.5 apparatus working at a constant traction speed of 1 mm. min^{-1}. Raman measurements were conducted on a dispersive Raman spectrometer, model NRS-3100 (Jasco), equipped with a confocal microscope. Photoluminescence measurements were performed at room temperature using the fourth harmonic (266 nm) of a Brilliant (Quantel) Q-switched Nd:YAG laser as the excitation source. The laser pulse frequency was 5 Hz, and the pulse duration around 4–6 nanosec. Fluorescence was detected with a StellarNet EPP2000-UV-VIS spectrometer.

3. Results and Discussion

3.1. Fibers Preparation

As shown in **Figure 1**a, the ZnO particles present a significant anisotropic shape with an aspect ratio, length/diameter, of around 20. This shape ratio would formally rank these particles among the "nanowire" nomenclature, but we think that the "nanorod" terminology remains more appropriate and descriptive. The other composite fibers that had been prepared until now with the micro-extrusion method, used particles with a much higher aspect ratio,[14,15,19] and the method was based on the co-injection of the inorganic phase along with the PVA gelling agent into an aqueous solution of PVA that polymerized around the extruded flow. This method could not be applied straightforwardly with the present system, probably because of the restricted aspect ratio of ZnO particles, compared with V_2O_5 ribbons and CNT. As a result, we turned the synthetic

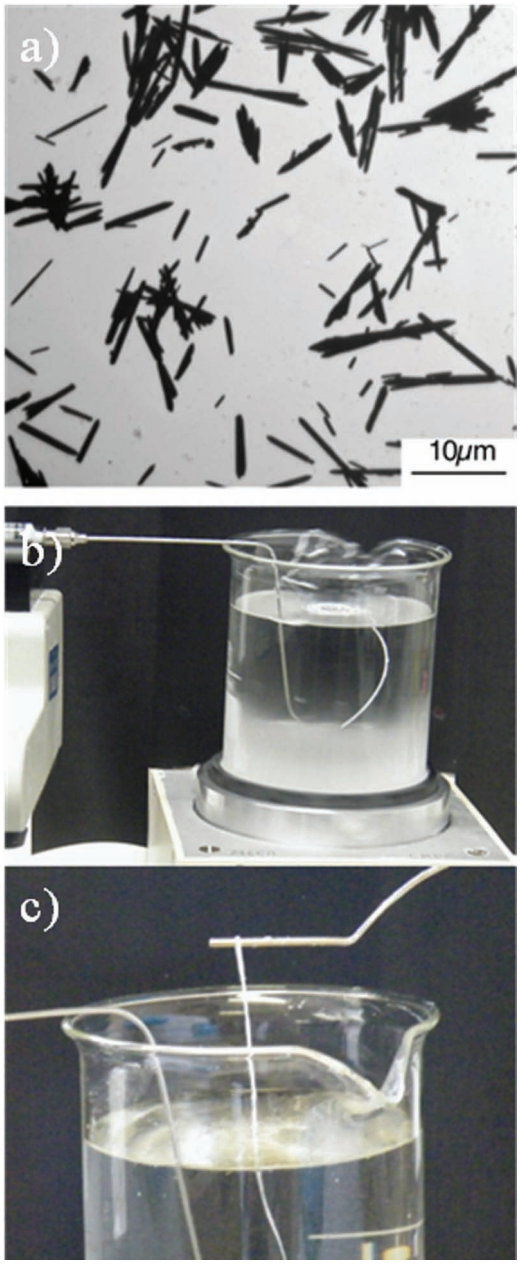

Figure 1. Overall synthetic path. a) as-synthesized TEM picture of ZnO particles b) typical extrusion where the PVA/ZnO hybrid sol is injected through a syringe needle into a rotating beaker containing a Na_2SO_4 saturated water solution. c) as-synthesized hybrid fibers extracted by hand from the beaker.

route toward a new scenario where the PVA is injected with the nanoparticles into a beaker containing the gelling agent, that is, a saturated aqueous solution of Na_2SO_4 (Figure 1b). This new method allowed us to obtain PVA/ZnO composite fibers, that present a crude mechanical resistance high enough to allow their extraction by hand (Figure 1c) before washing and air drying.

Table 1. Elemental Analysis.

Element	C	Zn	Na
wt% (exp.)	23,3	28,4	6,6
wt% (cal.)	24,5	30,3	7,4

3.2. Fibers Characterization

The water content and organic/inorganic matter composition of the composite fibers was deduced from TGA experiments (Supplementary Info figure 1S). The TGA curves present a first weight loss of 1.5 wt% between ambient temperature and 200 °C, which corresponds to hydration water, followed with a weight loss of 45 wt% between 250 °C and 500 °C, resulting from the organic matter calcination, from which a 55:45 inorganic:organic mass ratio is deduced. The initial analysis was completed with C, Zn and Na elemental analyses, which allowed us to refine the amount of sulfate, PVA and sodium present in the fibers. From the combination of both TGA and elemental analyses (**Table 1**), the following fibers stoichiometry is proposed: $(ZnO)(PVA)_{2.2}(Na_2SO_4)_{0.35}.0.2H_2O$. Considering the proposed composition we notice that a significant amount of sodium sulfate remains trapped in the composite fibers, despite severe washing, as evidence below with XRD investigations. This salt is embedded within the PVA matrix as a result of its polymerization.

The crystalline structure of the ZnO particles was characterized by XRD (**Figure 2**b). The ZnO nanorods present the hexagonal ZnO Wurtzite (space group $P6_3mc$) structure with lattice constants a = 3.25(2) Å and c = 5.21(2) Å, in good agreement with the expected values (JCPDS 76–0704). The XRD pattern of the composite fibers (Figure 2d) was compared with that of PVA (Figure 2a) and Na_2SO_4 (Figure 2c). The diffractogram confirms the combination of ZnO and PVA, with the sodium sulfate embedded in the fiber.

The crystalline structure of the ZnO particles was further investigated by Raman scattering to evaluate the level of

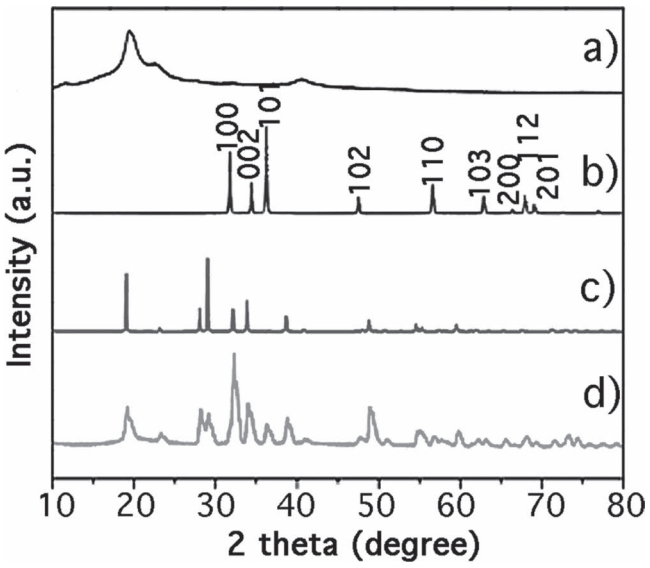

Figure 2. X-rays diffraction patterns of a) PVA, b) ZnO, c) Na_2SO_4 salt and d) composite PVA/ZnO fibers.

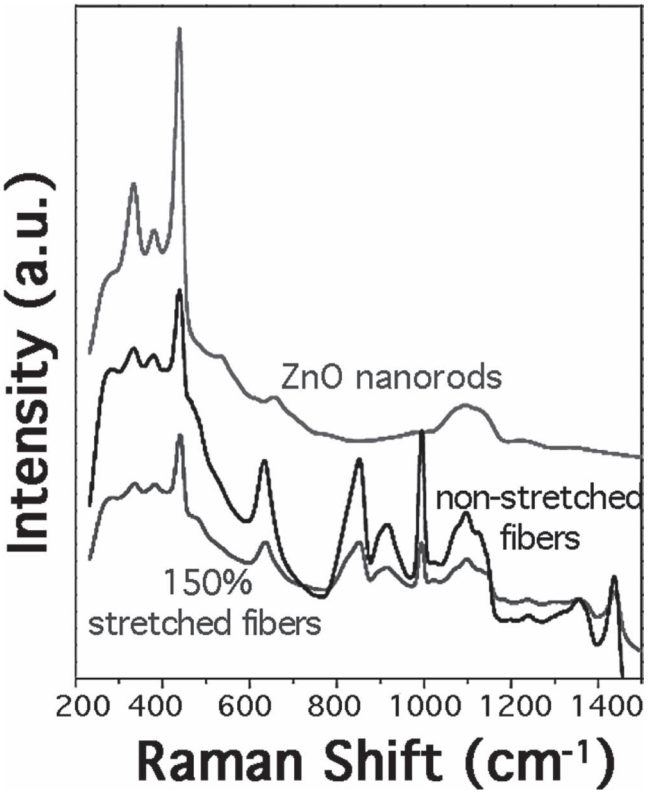

Figure 3. Raman spectra of the ZnO nanorods (Top), non-elongated PVA/ZnO fibers (Middle) and 150% - elongated PVA/ZnO fibers (Bottom) excited by 785 nm line. The symbol W indicates vibration modes induced by the ZnO inorganic Wurtzite structure; the stars indicate vibration modes associated to the PVA counterpart.

crystallinity and concomitantly that of defects (**Figure 3**). The Raman spectrum is characteristic of pure and well-crystallized hexagonal wurtzite:[20] it is mostly dominated by a sharp peak at 438 cm^{-1} attributed to the E_{2H} mode, but other weaker peaks are observed at 335, 381 and 1095 cm^{-1}, which correspond to the E_{2H}-E_{2L}, A_{1T} multiphonon contributions, and the acoustic combination of A_1 and E_2 modes, respectively. The absence of contribution around 578–583 cm^{-1} (A_{1L} and E_{1L} modes) reveals the absence of punctual defects such as interstitial zinc cations or oxygen vacancies, in the ZnO lattice.[21] The spectra of the ZnO fibers indicate that ZnO structure remains unchanged upon extrusion, and that no significant defects associated to the extrusion process have been created. However, compared with the ZnO particle alone, the Raman spectra of the composite fibres show a slight blue shift of the peak at 438 cm^{-1}, corresponding to the E_{2H} mode. This E_{2H} mode is usually used to probe the degree of crystalline stress of the ZnO crystals,[22] and the E_{2H} frequency of the Wurzite ZnO crystal is blue-shifted when submitted to pressure, this variation being assigned to changes in the content of defects (oxygen vacancies, etc…).[23] In our study, a small blue-shift of less than 2 cm^{-1} was detected for the elongated ZnO fibers, which we ascribe to a minor stress induced by the PVA matrix confinement onto the ZnO nanocrystals when the fibre is stretched out.

Integration of ZnO nanorods into PVA fibers was carried out to explore how the preferential alignment along a single main axis could amplify the mechanical and photonic properties of the resulting material by providing some collective anisotropy as a result of a preferential alignment of the ZnO nanorods. Such an effect was already observed with V_2O_5/PVA composite fibers,[16] and it depends on the extrusion shear rate. As the shape factor of ZnO particles is smaller than that of V_2O_5 ribbons, the alignment of the ZnO particles had to be improved by stretching the composite fibers, at a temperature above the PVA glass transition temperature (around 70 °C for Mw = 120 000). Depending on the hydration state, Tg can vary within 69 °C–72 °C (see DSC analysis in SI. Figure 2S), and we proceeded to the mechanical fiber extension at 85 °C. SEM observation (**Figure 4**) confirms that the fiber stretching promotes a better alignment of the ZnO particles along the fiber main axis.

Without the fiber pre-stretching, a spontaneous but limited pre-alignment of the ZnO particles exists (Figure 4a,b), as a result of the co-axial flux shaping extrusion, but this alignment remains limited. Applying tensile stress to the fiber above the PVA T_g and cooling it down under stress, drastically increases this alignment (Figure 4c,d), as confirmed by SAXS/XRD. The experimental geometry was set in order to detect reflections up to ($2\cup = 40°$), that is, an angular range containing the three main reflections of the wurtzite structure: (00l), (002), and (101) (**Figure 5**) (additional reflections due to the Na_2SO_3 salt are also observed). This pattern was collected with a slightly stretched fiber and the angular distribution of the scattered intensity gives access to quantitative information on the angular distribution of the main axis of the ZnO nanorods.

This diffraction pattern reveals the anisotropic distribution of the intensity corresponding to the (00l), (002), and (101) planes. With a fiber vertically placed and perpendicular to the X-ray beam, the maximum of intensity is centred on the coronal and sagittal planes for the (100) and (002) reflections, respectively. As for the diffraction assigned to (101), it is distributed over four spots at $\pi/4$ of the coronal and sagittal planes (Figure 5). We selected the (100) reflection line to quantify the angular distribution χ of the diffracted intensity $I = f(\chi)$. As illustrated with the wo examples reported in **Figures 6**(a) and (b), for non elongated and 150% elongated fibers, respectively, the intensity as function of the angular distribution, is narrower for the elongated fiber than for the non-elongated one, as a result of a better alignment among the ZnO nanorods.

Each intensity profile was fitted with a Lorentzian function and the full width at half maximum (FWHM) of this curve was used to quantify the degree of anisotropy among a group of fibers that had been stretched under different extension stress (Figure 6c): the smaller the FWHM, the higher the alignment. Figure 6c presents the evolution of FWHM/2 versus the elongation percentage of the fibers. As already observed on SEM images, the ZnO particles are already partially aligned by the extrusion process with an average angle of ±31° with respect to the fiber axis. This alignment is improved upon fiber stretching with a limit reached for 100%- elongated-fibers. Above 100% extension the ZnO wires mean orientation within the fibers is no more improved. This result was confirmed with similar analyses carried out on several set of fibers.

Fibers mechanical properties. A preliminary test revealed that these composite fibers can stand a tight knot formation

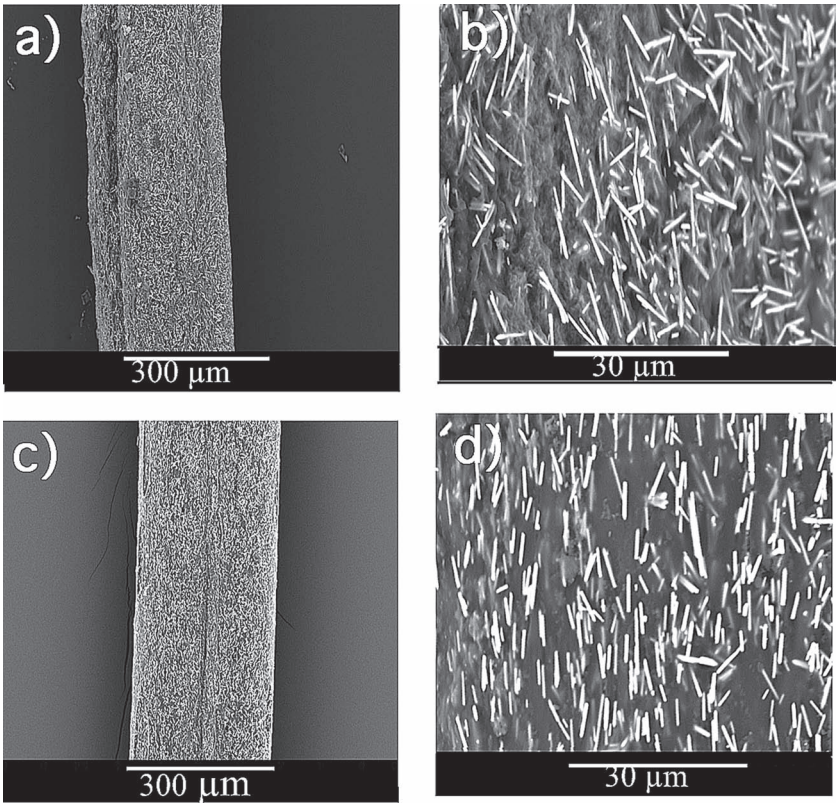

Figure 4. SEM images of a non-elongated fibers (a, b) and of a 150%-elongated fiber (c, d). The white arrows indicate the fibers axis.

(**Figure 7**), which confirms that they posses good mechanical properties in terms of both transversal flexibility and the absence of longitudinal plasticity.

More accurate tests were carried out with fibers prepared with different post-synthesis stretching. As illustrated in **Figure 8**, that displays the different tensile stress curves as a function of the applied extension strain, non-extended fibers exhibit only an elastic behavior with a reversible strain up to 2% before rupture. As the fiber is pre-stretched at 50%, its mechanical properties are modified with an additional plastic response that allows for an additional 8% non-reversible strain. Extension of the pre-stretching to 100% increases the tensile strength resistance since the elastic limit is reached for a higher stress (50 MPa instead of 25 MPa for the non-extended fiber). Finally, higher pre-extension (150%) has a negative impact on the stress/strain curve, probably as a result of a too extensive fiber extension that degrades the PVA matrix cohesion. These tests along with the macroscopic behavior as illustrated in Figure 7, illustrate the synergy between the two components (PVA, ZnO): (i) PVA provides the organic flexibility to the inorganic part and confines the ZnO nanorods within a compressive matrix, as revealed by the Raman analysis, and (ii) the ZnO nanorods provide an additional resistance via their intrinsic mechanical strength and the collective resistance resulting from their preferential alignment along the PVA fiber main axis. An additional proof of the constriction of the PVA matrix around the ZnO nanorods, as a result of the pre-extension, is the increasing of the nanocomposite fiber stiffness marked by an important improvement of the Young Modulus (**Table 2**).

In the elastic regime, at low strain, the tensile Young modulus varies from 2 to 6 GPa as the post-synthesis fiber extension goes from 0 to 100% extension, which corresponds to the range of values obtained for similar composite fibers, prepared either with carbon nanotubes[15] or V_2O_5.[14] Here again, increasing the fiber extension beyond 100% has a negative impact on the Young Modulus.

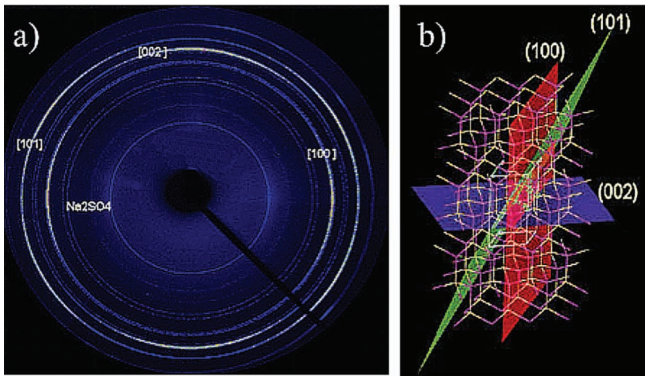

Figure 5. a) 2D X-Ray pattern of a partially elongated fiber. The fiber axis is vertical. b) unit cell of the wurtzite (space group P63mc) with the visualization of the crystallographic planes of interest.

3.3. Fibers Photonic Properties

We conducted photonic analyses on ZnO fibers since ZnO photoluminescence significantly varies depending on the quality of the crystals and the presence and nature of defects (oxygen vacancies, interstitial zinc cations, etc…). The control of defects is indeed of paramount importance in applications that exploit the wide range of optoelectronic properties. Photonic properties of ZnO are well known, and we focused our analysis on the influence of both the intrinsic ZnO particle anisotropy and collective alignment onto the optical properties. Therefore, the optical measurements were designed in order to see how both dimensionality and alignment of nanorods along the fiber main axis, influence the photonic properties. Measurements were carried out first in two configurations: (a) laser beam perpendicular, that is, at an angle of 90°, to the fiber main axis (Electrical field parallel to the plane of the fiber main axis), and (b) laser beam parallel, that is, at an angle of 0°, to the fiber main axis (Electrical field perpendicular to the fiber main axis), (see **Scheme 1**). These two configurations were used to measure the photoluminescence resulting from

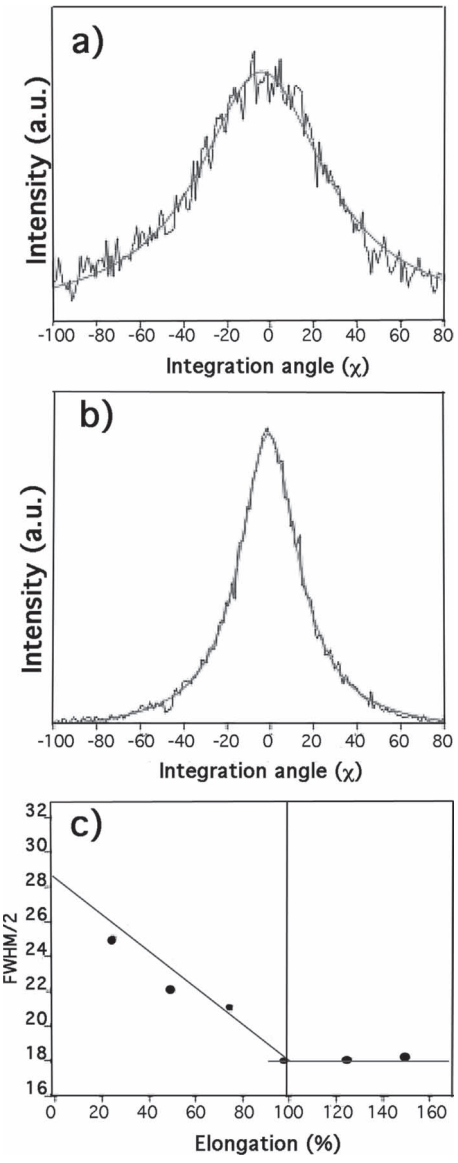

Figure 6. (a,b) Curves representing the Lorentzian integration of the light intensity on the circle corresponding to the (100) diffraction and their fitting, (a) non-elongated fibers, (b) 150%-elongated fiber; (c) presents the FWHM/2 evolution of the fitted peaks, as a function of the stretching percentage.

the anisotropic absorption for non-stretched (Scheme 1a) and stretched (Scheme 1b) fibers.

Figure 9a displays the photoluminescence (PL) spectra obtained for the non-stretched fibers with the laser oriented at 90° or 0° of the fiber main axis. Their photoluminescence is compared with that of ZnO particles alone. The PL spectrum of ZnO particles is dominated by a sharp and strong peak at around 388 nm (3.27 eV) in the UV region. This emission corresponds to the near band edge emission (NBE) of highly pure wurtzite ZnO crystals, and it arises from the recombination of the free excitons through an exciton–exciton collision process. This band presents a shoulder at lower energies (lambda > 390 nm), which it is usually assigned to optical transitions involving free electrons and neutral-acceptor levels. The contribution of each of both signals was obtained by deconvolution of the spectra (see **Table 3**). No other signals in the green visible region (450–600 nm) associated to defects or impurities were detected.[22–24]This profile in the PL spectrum confirms that the ZnO structure is highly crystalline with no structural defects, in agreement with SEM, WAXS and XRD results.

The luminescence spectra of the nanocomposites ZnO-PVA fibers display similar, but broader, profiles as for the ZnO particles alone. This broadening results from surface interactions between free electrons on the ZnO surface and the polymer matrix. For non-stretched fibers, a similar response is observed for both the longitudinal and transversal measurements. This isotropic response illustrates the poor alignment of ZnO nanorods after the fiber extrusion if the post-extrusion stretching is not applied. On the contrary (Figure 9b), responses of stretched fibers display huge differences: the intense UV emission detected when the laser beam is perpendicular to the fiber main axis (90°) is almost suppressed when the measurement is conducted with the laser beam parallel to the fiber main axis (0°). This difference can result only from the alignment of ZnO nanorods within the composite fiber, and their resulting orientation with the incident beam. If the propagation vector $\vec{k}$ of the incident light is normal to the fiber and concomitantly to the aligned ZnO nanorods main axis, then the light wave, polarized with its electric field $\vec{E}$ (perpendicular to $\vec{k}$) parallel to the axis of the fiber will gives an optimal interaction with the absorption transition dipole of ZnO ($\vec{\mu}_{ZnO}$), and $\vec{E}.\vec{\mu}_{ZnO}$ will be maximal. If the propagation vector $\vec{k}$ of the incident light is parallel to the main axis of the fiber, then $\vec{E}.\vec{\mu}_{ZnO}$ is almost equal to zero, and almost no PL will be detected.

In addition to enhanced photoluminescence,[25] it is expected that spatially aligned 1D ZnO nanostructures can exhibit polarized emission,[9] or photonic confinement.[26] The size scale for reaching quantum confinement and waveguiding phenomena is close to the average Bohr radius for excitons in ZnO, and this value has not yet been attained in the synthesis of single-ZnO crystalline wires. We determined if the preferential orientation of ZnO nanorods inside the polymer provided some of these particular photonic effects as a result of their collective response. The small diameter of the fibers (~1 mm) prevented us from recording the PL emission as a function of several angles with our current system. Therefore, we positioned the detector at two positions (**Scheme 2**), toward the side of the fiber, at 90° of the laser (position 1), or toward the cross-section of the fiber at 90° of the laser (position 2).

The laser beam was polarized with the electric field parallel to the main axis of the fiber in order to assure an optimal interaction with the absorption dipole of ZnO. The measurements have been conducted with identical experimental conditions, and special care was taken to ensure that no reflected incident beam was hitting the detector. The spectra were finally normalized in order to compare the intensity of the signals. **Figure 10** shows the emission spectra registered for the composite fibers without (a) or with (b) elongation.

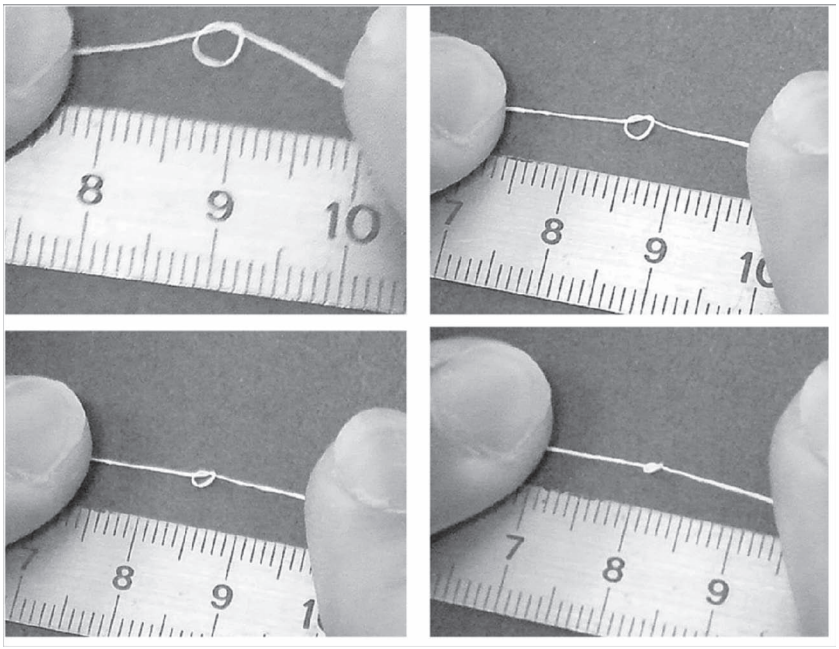

Figure 7. Sequenced pictures showing ZnO non-elongated fibers forming a tight knot.

As PL emission is isotropic, its angular dependence mostly depends on the surface of emission in a given direction. Hence, the emission is enhanced perpendicularly to the main axis of the nanorods, because the surface of emission is larger, compared to the cross-section of the fiber. It is also expected that the collective alignment of ZnO nanorods in the PVA fibers, should give an anisotropic angular emission with two major angles of emission: perpendicular to the fiber, since the surface of emission of the ZnO nanorods is larger, and along the fiber main axis, as a result of the anisotropy of alignment of the ZnO nanorods. The comparisons between the PL spectra upon polarized light excitation for the non-stretched and stretched fibers, show indeed that the intensity of the emission by non-stretched fibers, is more homogeneously distributed than for the stretched ones. For example, the emission perpendicular to the fiber (detector in position **1**) is enhanced with the stretched fiber (Figure 10b), compared to the non-stretched one (Figure 10a). More important, the non-stretched fiber does not emit any PL along the main axis of the fiber (detector in position **2**) (Figure 10b) whereas the stretched one (Figure 10a) demonstrates a clear PL emission. Moreover, we observed that the luminescence peak shifts slightly from 388.5 to 386.9 nm when the detector is changed from position **1** to **2**. This blue-shift has already been observed in other aligned anisotropic ZnO nanostructures.[27] It has been assigned to a surface effect, because the mechanism accounting for this energy shift is the concentration of native defects on the surface area.[28] With the ZnO particle size decreasing, the surface-to-volume ratio increases and surface phenomena become preponderant. It is then inferred that the energy shift in all the excitonic transitions of the nanorods is due to the influence of the total surface area made available by alignment of the ZnO nanorods. Thus, the energy of the band-edge transition in the PL spectrum of stretched fiber is higher than that of non-stretched one due to the larger additional surface area of the lateral planes $\{10\bar{1}0\}$ in the aligned ZnO fiber than those of the top planes {0001} in the non aligned ZnO fiber. Additionally, tests to detect photonic confinement and an actual waveguide phenomenon were not conclusive with our experimental system setup: the presence of flat and parallel end faces on the nanowires is a requirement for the optical feedback in a resonant cavity, and this feature is very difficult to reach when nanorods are interacting with a polymer host matrix. However, our measurements demonstrate that the parallel alignment of ZnO nanorods along the PVA fiber main axis allows the nanorods to act collectively as an antennae with polarized optical emission. This particular alignment provides preferences in the PL emission directions, which should be enhanced by a still higher alignment of nanorods within the PVA matrix.

4. Conclusion

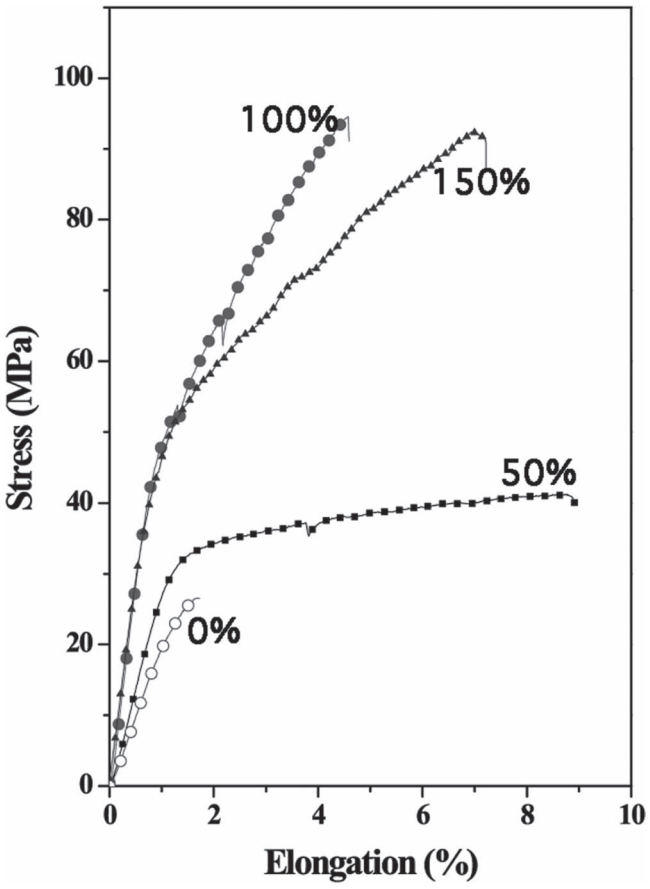

Figure 8. Mechanical tests on fibers elongated at several percentages: ○ not extended, ■ 50%, ● 100%, ▶ 150%.

Table 2. Mechanical properties of fibers stretched at different percentages (values have been normalized to the fiber section).

elongation%	Young Modulus (GPa)	Tensile strength (MPa)
0	2,0	39,6
50	3,2	43,4
100	6,0	79,9
150	5,2	79,2

Composite macroscopic fibers made of ZnO nanorods embedded into PVA matrix have been synthesized through coaxial flux nanoparticles alignment, with a modified process, compared with previous studies. Unlike other works where the very high aspect ratio of particles allowed for an easy alignment during the fiber extrusion, the correct alignment of the ZnO particles could be achieved only with a specific post-synthesis fiber stretch process under hot mechanical traction above the polymer glassy transition temperature. The as-synthesized fibers have been thoroughly characterized at the macro-, meso and microscopic length scales. According to the XRD pattern, ZnO corresponds well with hexagonal ZnO Wurtzite-type (space group $P6_3mc$) with lattice constants a = 3.25 Å and c = 5.21 Å. Raman spectroscopy has revealed that the ZnO particles exhibit a high crystallinity, and no significant defects associated to the extrusion process were observed. A small blue-shift of less than 2 cm^{-1} was detected for the elongated ZnO fibers, which reveals that the fibre extension process improves the interaction between the polymer matrix and particles, and creates locally some surface stress in the ZnO structure. At the mesoscopic length scale, the ZnO nanorods

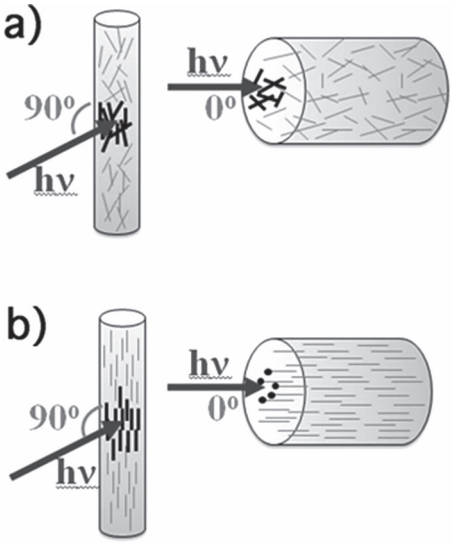

Scheme 1. Schematic representation of PL measurements on non-stretched (left) and stretched (right) ZnO fibers. The excitation beam strikes perpendicularly to the ZnO fiber (angle of 90°, configuration a) and parallel to the ZnO fiber (angle of 0°, configuration b), and detector is place at an angle of 45° between the laser and the main axes of the fibers.

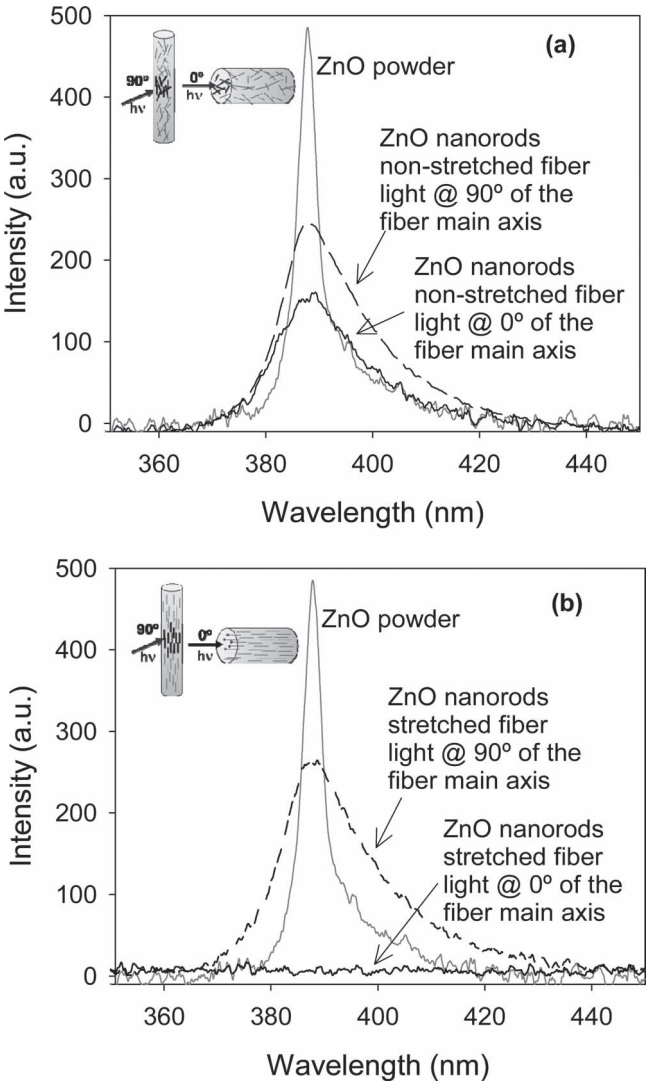

Figure 9. PL spectra of (a) non-stretched and (b) stretched ZnO fibers measured upon excitation beam oriented at 90° (configuration a, Scheme 1) and 0° (configuration b, Scheme 1). The grey plain curve corresponds to the PL spectrum of pure ZnO nanorods (reference).

are partially pre-aligned by the extrusion process itself with an average angle of 31 degrees, but this alignment is not high enough to emphasize anisotropic properties. Improvement of

Table 3. Contribution of each signal (mean peak at ~380 nm and the shoulder at ~390 nm) to the total emission spectra in different samples. The 380 nm peak corresponding to the recombination of free excitons through an exciton–exciton collision process and the ~390 nm peak to optical transitions involving free electrons and neutral-acceptor levels.

Sample	% (380 nm)	% (390 nm)
ZnO nanorods	63	37
ZnO/PVA fiber (non stretched)	48	52
ZnO/PVA fiber (150% stretched)	51	49

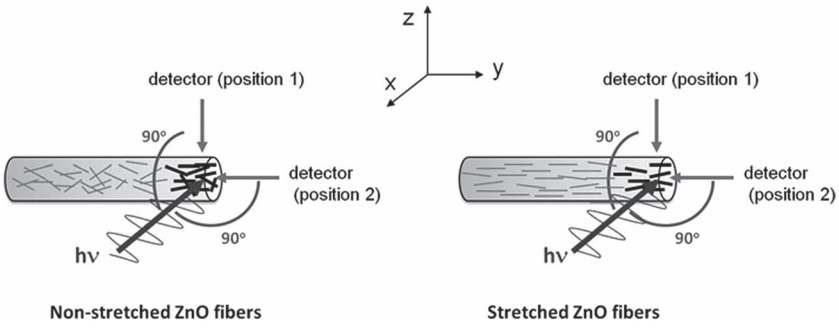

Scheme 2. Schematic representation of PL measurements on non- stretched (left) and stretched (right) ZnO fibers. The excitation beam strikes perpendicularly to the ZnO fiber (angle of 90°) and the detector is positioned in two perpendicular directions to the incident laser.

this alignment through the applied hot mechanical traction step allowed us to confine the mean alignment of nanorods within a 18° angle value at 100% elongation, above which ZnO wires main orientation within the fibers remains constant. Considering these fibers mechanical properties we have found that the longitudinal Young's modulus can be increased from 2 to 6 GPa. When photonic properties are addressed, intense near band edge (NBE) emission with no green emission in the PL spectrum confirmed that the ZnO particles are highly crystalline with no structural defects. In the case of non-elongated fibers, an isotropic response was observed in the longitudinal and transversal measurements. On the contrary, for elongated fibers, the intense UV emission detected when the ZnO nanorods are aligned perpendicular to the laser beam is almost suppressed when the measurement is conducted at an angle of 0º, depicting thereby anisotropic photonic properties. Similar anisotropy was observed regarding the angular dependence of the photoluminescence emission.

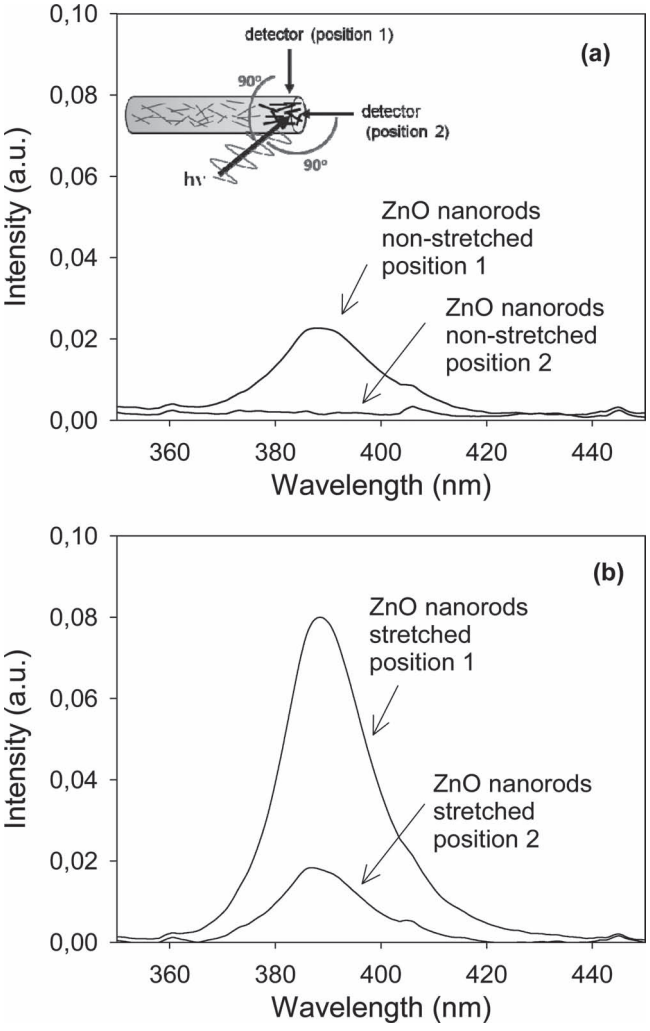

Figure 10. PL spectra of (a) non-stretched and (b) stretched ZnO fibers obtained with polarized excitation beam, and detection according to the setup of Scheme 2 (detector position 1 Top, and detector position 2 Down).

Supporting Information

Supporting Information is available from the Wiley Online Library or from the author.

Acknowledgements

We thank Prof. Gilles Sigaud for his help in acquiring the DSC data. We also wish to thank European Union and the IDS-FunMat consortium for funding of N. K. PhD scholarship, and management of the associated European training program. B. J. -L. is especially thankful to Spanish Government and Bancaixa-UJI for funding this research ("Ramón y Cajal" contract, MAT 2008-03479, MAT2011-27008, and P1 1B2010-36 projects). E. P. thanks the Canadian NSERC Agency for funding through the "Discovery Grants". This article was modified on October 10, 2012 to correct typographical errors on page 3999 that were present in the version originally published online.

Received: February 6, 2012
Published online: June 5, 2012

[1] Z. L. Wang, *Mater. Today* **2004**, *7*, 26.
[2] M. H. Huang, S. Mao, H. Feick, H. Yan, Y. Wu, H. Kind, E. Weber, P. Russo, P. Yang, *Science* **2001**, *292*, 1897.
[3] A. Umar, H.-W. Ra, J.-P. Jeong, E.-K. Suh, Y.-B. Hahn, *Korean J. Chem. Engin.* **2006**, *23*, 499.
[4] A. Umar, S. H. Kim, Y. S. Lee, K. S. Nahm, Y.-B. Hahn, *J. Cryst. Growth* **2005**, *282*, 131.
[5] W. L. Hughes, Z. L. Wang, *Appl. Phys. Lett.* **2003**, *82*, 2886.
[6] B. P. Zang, N. T. Binh, K. Wakastuki, Y. Segawa, Y. Yamada, N. Usami, H. Koinuma, *Appl. Phys. Lett.* **2004**, *84*, 4098.
[7] G. Shen, Y. Bando, B. Liu, D. Golberg, C.-J. Lee, *Adv. Funct. Mater.* **2006**, *16*, 410.
[8] a) R. E. Dietz, D. G. Thomas, J. J. Hopfield, *J. Appl. Phys.* **1961**, *32*, 2282; b) A. Mizukoshi, J. Ozawa, S. Shirakawa, K. Nakano, *Ieee Trans. Power Apparatus Systems* **1983**, *102*, 1384; c) D. Fichou, J. Kossanyi, *J. Electrochem. Soc.* **1986**, *133*, 1607.
[9] S. Baskoutas, G. Bester, *J. Phys. Chem. C* **2011**, *115*, 15862.
[10] C.-T. Chien, M.-C. Wu, C.-W. Chen, H.-H. Yang, J.-J. Wu, W.-F. Su, C.-S. Lin, Y.-F. Chen, *Appl. Phys. Lett.* **2008**, *92*.

[11] a) R. Backov, *Soft Matter* **2006**, *2*, 452; b) E. Prouzet, S. Ravaine, C. Sanchez, R. Backov, *New J. Chem.* **2008**, *32*, 1284; c) R. Backov, *Actualité Chimique* **2009**, *329*, III.
[12] a) S. Mann, *J. Mater. Chem.* **1995**, *5*, 935; b) C. Sanchez, H. Arribart, M.-M. Giraud Guille, *Nat. Mater.* **2005**, *4*, 277.
[13] a) N. Brun, S. Ungureanu, H. Deleuze, R. Backov, *Chemical Society Reviews* **2011**, *40*, 771; b) E. Prouzet, Z. Khani, M. Bertrand, M. Tokumoto, V. Guyot-Ferreol, F. Tranchant, *Microporous Mesoporous Mater.* **2006**, *96*, 369; c) F. Carn, A. Colin, M.-F. Achard, H. Deleuze, E. Sellier, M. Birot, H. Deleuze, R. Backov, *J. Mater. Chem.* **2004**, *14*, 1370; d) F. Carn, A. Colin, M.-F. Achard, H. Deleuze, C. Sanchez, R. Backov, *Adv. Mater.* **2005**, *17*, 62; e) M. Destribats, V. Schmitt, R. Backov, *Langmuir* **2010**, *26*, 1734; f) N. Brun, S. R. S. Prabahan, M. Birot, C. Sanchez, M. Morcrette, G. Pécastaing, A. Soum, H. Deleuze, R. Backov, *Adv. Funct. Mater.* **2009**, *19*, 3136; g) N. Brun, A. Babeau-Garcia, M.-F. Achard, C. Sanchez, F. Durand, L. Guillaume, M. Birot, H. Deleuze, R. Backov, *Energy Environm. Sci.* **2011**, *4*, 2840.
[14] L. Biette, F. Carn, M. Maugey, M.-F. Achard, J. Maquet, N. Steunou, J. Livage, H. Serier, R. Backov, *Adv. Mater.* **2005**, *17*, 2970.
[15] B. Vigolo, A. Penicaud, C. Coulon, C. Sauder, R. Pailler, C. Journet, P. Bernier, P. Poulin, *Science* **2000**, *290*, 1331.
[16] H. Serier, M.-F. Achard, O. Babot, N. Steunou, J. Maquet, J. Livage, C. M. Leroy, O. Babot, R. Backov, *Adv. Funct. Mater.* **2006**, *16*, 1745.
[17] a) J. Dexmer, C. M. Leroy, L. Binet, H. Heresanu, P. Launois, N. Steunou, C. Coulon, J. Maquet, N. Brun, J. Livage, R. Backov, *Chem. Mater.* **2008**, *20*, 5541; b) C. M. Leroy, M.-F. Achard, O. Babot, N. Steunou, P. Massé, J. Livage, L Binet, N. Brun, R. Backov, *Chem. Mater.* **2007**, *19*, 3988; c) N. Brun, C. Leroy, H. Serier, J. Dexmer, F. Carn, R. Backov, *Comptes Rendus Chimie* **2010**, *13*, 154.
[18] H. Zhu, D. Yang, H. Zhang, *Inorg. Mater.* **2006**, *42*, 1210.
[19] a) P. Miaudet, S. Badaire, M. Maugey, A. Derré, V. Pichot, P. Launois, P. Poulin, C. Zakri, *Nano Lett.* **2005**, *5*, 2212; b) P. Miaudet, A. Derré, M. Maugey, C. Zakri, P. M. Piccione, R. Inoubli, P. Poulin, *Science* **2007**, *318*, 1294; c) C. Mercader, A. Lucas, A. Derré, C. Zakri, S. Moisan, M. Maugey, P. Poulin, *Proc. Natl. Acad. Sci. U.S.A.* **2010**, *107*, 18331.
[20] a) S. S. Mitra, J. I. Bryant, *J. Phys.* **1965**, *26*, 610; b) J. M. Calleja, M. Cardona, *Phys. Rev. B* **1977**, *16*, 3753.
[21] A. Umar, S. H. Kim, J. H. Kim, Y. K. Park, Y.-B. Hahn, *Mater. Lett.* **2007**, *61*, 4954.
[22] C. Li, G. Hong, P. Wang, D. Yu, L. Qi, *Chem. Mater.* **2009**, *21*, 891.
[23] F. Decremps, J. Pellicer-Porres, A. M. Saitta, J.-C. Chervin, A. Polian, *Phys. Rev. B* **2002**, *65*.
[24] X. Wang, K. Huo, F. Zhang, Z. Hu, P. K. Chu, H. Tao, Q. Wu, Y. Hu, J. Zhu, *J. Phys. Chem. C* **2009**, *113*, 170.
[25] S. Chawla, N. Karar, H. Chander, *Phys. B-Condensed Matter* **2010**, *405*, 198.
[26] a) J. C. Johnson, H. Yan, P. Yang, R. J. Saykally, *J. Phys. Chem. B* **2003**, *107*, 8816; b) X. Wang, C. J. Summers, Z. L. Wang, *Nano Lett.* **2004**, *4*, 423.
[27] C.-H Hoa, J.-S. Li, Y.-J. Chena, C.-C. Wua, Y.-S. Huang, K.-K. Tiong, *J. Alloys Comp.* **2009**, *480*, 50.
[28] A. B. Djurisic, Y. H. Leung, *Small* **2006**, *2*, 944.